JOURNAL OF NEUROTRAUMA 36:1389–1398 (May 1, 2019)
© Mary Ann Liebert, Inc.
DOI: 10.1089/neu.2018.5964

Original Articles

Longitudinal *In Vivo* Diffusion Magnetic Resonance Imaging Remote from the Lesion Site in Rat Spinal Cord Injury

Alice Motovylyak,[1] Nathan P. Skinner,[2,3] Brian D. Schmit,[1] Natasha Wilkins,[2] Shekar N. Kurpad,[2] and Matthew D. Budde[2]

Abstract

Diffusion tensor imaging (DTI) has demonstrated success as a biomarker of spinal cord injury (SCI) severity as shown from numerous pre-clinical studies. However, artifacts from stabilization hardware at the lesion have precluded its use for longitudinal assessments. Previous research has documented *ex vivo* diffusion changes in the spinal cord both caudal and cranial to the injury epicenter. The aim of this study was to use a rat contusion model of SCI to evaluate the utility of *in vivo* cervical DTI after a thoracic injury. Forty Sprague-Dawley rats underwent a thoracic contusion (T8) of mild, moderate, severe, or sham severity. Magnetic resonance imaging (MRI) of the cervical cord was performed at 2, 30, and 90 days post-injury, and locomotor performance was assessed weekly using the Basso, Bresnahan, and Beattie (BBB) scoring scale. The relationships between BBB scores and MRI were assessed using region of interest analysis and voxel-wise linear regression of DTI, and free water elimination (FWE) modeling to reduce partial volume effects. At 90 days, axial diffusivity (AD_{FWE}), mean diffusivity (MD_{FWE}), and free water fraction (FWF_{FWE}) using the FWE model were found to be significantly correlated with BBB score. FWE was found to be more predictive of injury severity than conventional DTI, specifically at later time-points. This study validated the use of FWE technique in spinal cord and demonstrated its sensitivity to injury remotely.

Keywords: diffusion tensor imaging; free water elimination; spinal cord injury

Introduction

Diffusion tensor imaging (DTI) has long been utilized in research settings to evaluate spinal cord injury (SCI), but a reliable outcome biomarker to guide clinical management and rehabilitation strategies at the early stage has not yet been realized. Standard clinical assessments of function during the acute stage (≤ 48 h) do not necessarily predict long-term outcome with sufficient accuracy.[1,2] Magnetic resonance imaging (MRI) is a mainstay of spinal cord injury diagnosis; however, standard relaxation-based measurements such as T1- and T2-weighted imaging are only modestly predictive of eventual outcome.[3] Thus, more sensitive techniques, such as diffusion-weighted imaging (DWI), are being utilized and show promise as markers of injury severity and extent following SCI.[4–8] This study examined the use of DTI as a predictor of injury remote from the lesion site.

Spinal cord imaging is challenging due to a number of factors, including the small size of the cord and its location away from the body surface and radiofrequency coils. In addition, DWI is particularly prone to artifacts due to cerebrospinal fluid (CSF) pulsation and motion, including respiration. In acute spinal cord traumatic injury, imaging at the lesion site is complicated by the presence of hemorrhage and vertebral column displacements that can further prevent high-quality imaging.[9] Follow-up imaging at the site of injury is further complicated by metal surgical stabilization hardware, which causes extreme susceptibility differences and is particularly disastrous for echo planar imaging (EPI) used by most DWI acquisitions. As an alternative to imaging at the site of injury, imaging remote from the site of injury has also demonstrated utility as a marker of injury severity. For example, anatomical imaging of spinal cord diameter or cross-sectional area remote from the lesion site has been clearly demonstrated to relate to functional outcomes.[10,11] DWI in the cervical cord following a lower cervical or thoracic injury has shown to be a reliable marker of spinal cord trauma in both human patients and animal models.[7,12–15] Although previous studies in an *ex vivo* model of SCI have demonstrated that sites remote from the injury reflect diffusion changes related to injury severity and functional outcome,[5,7,16,17] these effects have not been systematically examined *in vivo.* The goal of this study was to perform i*n vivo* imaging remote from the injury site using a similar experimental paradigm as prior *ex vivo* studies.

[1]Department of Biomedical Engineering, Marquette University/Medical College of Wisconsin, Milwaukee, Wisconsin.
[2]Department of Neurosurgery, [3]Medical Scientist Training Program, Medical College of Wisconsin, Milwaukee, Wisconsin.

DTI also has other potential complications. In the spinal cord, partial volume effects between the white matter and surrounding CSF complicate analysis and interpretation. Alternative models of diffusion weighted signal have been developed and utilized to reduce the influence of these intra-voxel contributions and have been reported to improve sensitivity for neurological injury. In particular, the free water elimination (FWE) mathematic framework[18] utilizes a two-compartment model to separate diffusion properties of neuronal tissue from the freely-diffusing CSF component. It has not been utilized in the spinal cord, but has been shown to be effective in the brain to minimize CSF contamination,[19] improve tractography reconstruction,[20] segment edema surrounding tumors,[18] improve sensitivity to markers in Alzheimer's disease,[21] monitor changes in substantia nigra in Parkinson's disease[22] and most recently, separate signal contribution from perfusing blood.[23] An additional benefit of implementing this scheme is a voxel-wise map of free water, which has potential to be used as a new contrast mechanism of vasogenic edema.

This study used a rat contusion model of SCI with varying degrees of severity to examine diffusion characteristics remote from the lesion site over time. Both DTI and FWE diffusion models were examined to assess their relationship with locomotor function. Additional efforts to minimize motion-induced EPI ghosting artifacts, along with spatial registration of spinal cord images to a common space, allowed voxel-wise statistical analysis to identify regional location of changes in the cord and their relationships to function.

Methods

Spinal cord injury procedure

Forty female Sprague–Dawley rats (250–300 g) were used for this experiment. The sample size was determined using a power analysis, which is described in the supplementary information section (available online at www.liebertpub.com/neu). Female rats were chosen due to lower incidence of urinary tract infections; however, future studies would benefit from including both male and female populations. Rats underwent a graded spinal cord contusion injury at the T8 vertebral level using the MASCIS impactor (W.M. Keck Center for Collaborative Neuroscience, Piscataway, NJ), which is a widely-used injury model for experimental SCI in rodents.[24–27] Rats were anesthetized with 4% inhaled isoflurane prior to the procedure, ensuring absence of leg flexion-withdrawal and corneal reflexes; 2.5% isoflurane was maintained during the procedure. The back was shaved and sterilized with povidone-iodine, and a longitudinal incision was made over the mid-thoracic region. After gently moving aside the muscle and placing retractors, the lamina at T8 was cut and removed to expose the cord. The rat was suspended with clamps and the impactor rod was placed on the spinal cord above T8. The contusion was performed by dropping the 10 g rod from a height of 12.5, 25.0, or 50.0 mm to induce a mild, moderate, or severe injury, respectively, with 10 animals in each severity condition. The trajectory of the falling rod, impact velocity, cord compression distance, time, and rate were recorded and were consistent with expected values. Cord compression (mm) was also used as a parametric measure of injury severity. Ten sham animals underwent a laminectomy with the weight briefly placed on the cord, but they did not experience the weight drop. After the injury, the muscles were sutured in layers.

After surgery, rats were placed on post-operative care, including twice-daily bladder expression, one dose of enrofloxacin (10 mg/kg subcutaneously; Bayer Healthcare LLC, Shawnee Mission, KS), buprenorphine hydrochloride (0.1–0.5 mg/kg subcutaneously; Rickitt Benckiser Health Care Ltd, Hull, U.K.), and 6 cc of lactated Ringer's solution. Animals were kept under post-operative care procedures until bladder function returned and no signs of infection or stress were evident. All rats survived the injury procedures, but two animals were euthanized prior to the final time-point due to complications.

Each week, the rats' functional post-injury motor behavior was assessed on the Basso, Beattie and Bresnahan (BBB) scale, following standard procedures,[28,29] as a measure of functional recovery and locomotion. Briefly, rats were placed on a flat, one-meter diameter surface and observed for 4 min. Hindlimb function was assessed according to the 0 to 21 BBB scoring where 0 is flaccid paralysis and 21 is normal gait. All animal procedures were approved by the Institutional Animal Care and Use Committees at the Medical College of Wisconsin, the Zablocki VA Medical Center, and Marquette University.

MRI

MRI was performed at 2, 30, and 90 days after the injury procedure on a Bruker 9.4 T Biospec System using a commercial 3.8 cm inner diameter quadrature Litz volume coil (Doty Scientific, South Carolina). Animals were placed prone in a custom head holder with ear bars to minimize motion as previously described.[30] A four-shot, diffusion weighted EPI acquisition (echo time [TE] = 28 msec; repetition time [TR] ≥1500 msec, varied by respiratory rate) was used with a $25.6 \times 25.6\,mm^2$ field of view, matrix of 128×128, and nominal spatial resolution of $0.20 \times 0.20\,mm^2$ with 3/4 partial Fourier sampling. Fourteen axial slices with a thickness of 1.0 mm and 0.75 mm gap were positioned perpendicular to the spinal cord main axis spanning vertebral segments C1 to C5 with the first slice consistently positioned at the junction of the cerebellum and medulla. The phase encoding direction was along the A-P axis. Fat saturation was achieved with a frequency-selective saturation pulse in addition to gradient reversal of the slice selection and refocusing pulses.[31] Diffusion weighting employed Stejskal-Tanner diffusion gradients along 30 unique diffusion directions[32] at b values of 250, 500, 1000, and 2000 sec/mm^2 with a gradient duration (δ) and separation (Δ) of 8.25 and 12.5 msec, respectively. Additional 15 non-diffusion-weighted images were collected. Three signal averages were used and the entire acquisition required approximately 1 h. T2-weighted rapid acquisition with relaxation enhancement (RARE) images were acquired with the identical spatial resolution at TE = 16, 48, and 80 msec, TR = 3500 msec, number of excitation = 4, RARE factor = 4.

MRI processing

The preprocessing pipeline (Fig. 1) included correction for EPI artifacts, motion and eddy currents, and spatial registration to a common coordinate frame using a combination of open-source and custom software. The EPI phase correction to minimize ghosting artifacts was based on the algorithm described by Chen and colleagues[33] using an automated, iterative adjustment of the constant and linear phase of multi-shot complex k-space, which maximized the image signal relative to the background using histograms (Fig. 2). To correct for motion and eddy currents, a version of the Spinal Cord Toolbox[34] was modified to perform iterative slice-by-slice corrections. Briefly, each diffusion-weighted image was spatially aligned to the mean of all other images, weighted by the angle between the current and all other diffusion weighting vectors, a procedure similar in principle to methods implemented in FMRI Software Library (FSL)[35] using increasing degrees of freedom from translation, rigid-body, and affine transformations and three full iterations.

Diffusion modeling and parameter maps were calculated on a voxel-by-voxel basis by fitting signal intensity to several models. The diffusion tensor model of Basser and colleagues[36] was fit according to:

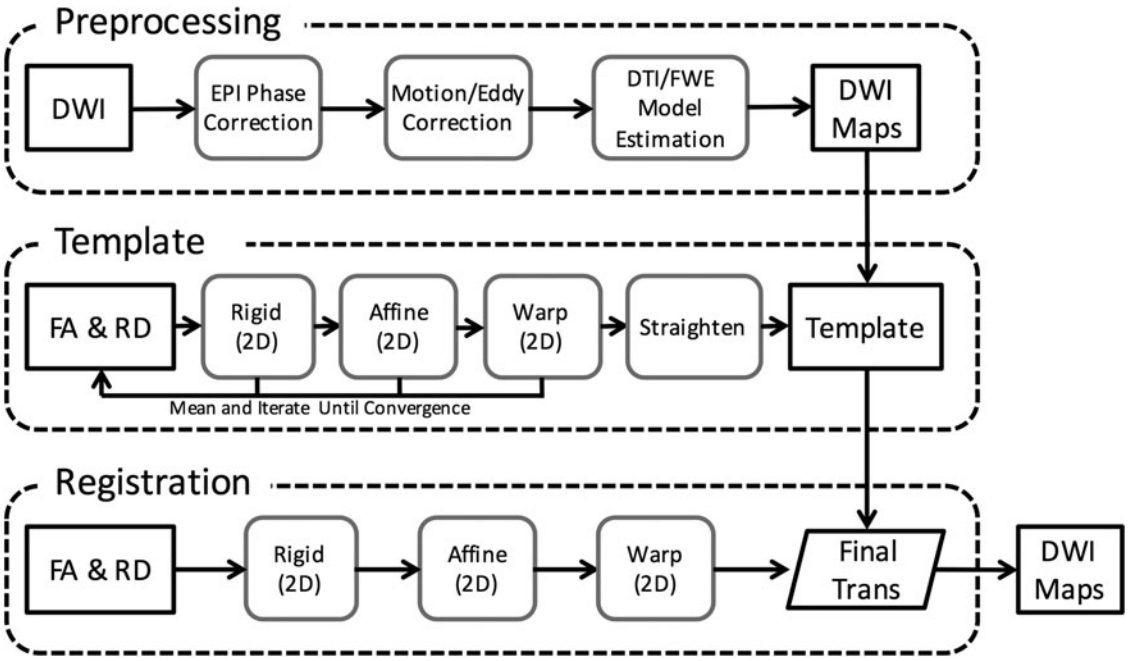

FIG. 1. Image analysis pipeline. Schematic representation of image preprocessing, including phase correction, and registration to template space for group-level analysis.

$$S_i = S_0 \cdot \exp(-bD) \quad [1]$$

where Si is the diffusion-weighted signal, S0 is the signal without diffusion encoding, D is the estimated diffusivity, and b is the strength of the diffusion weighting given by

$$b = \gamma^2 \cdot G^2 \cdot \delta^2 \left(\Delta - \frac{\delta}{3}\right) \quad [2]$$

The Free Water Elimination technique[18,19] used a two-compartment model to fit the diffusion signal where tissue and free water compartments are modeled as separate attenuation vectors, A, given as

$$A_{bi-tensor}(D, f) = fA_{tissue}(D) + (1-f)A_{water} \quad [3]$$

and f is the volume fraction of the tissue and D is the diffusion tensor. The Free Water Fraction (FWF) is calculated as 1-f. Since multiple b-value images were used, no spatial regularization was employed.

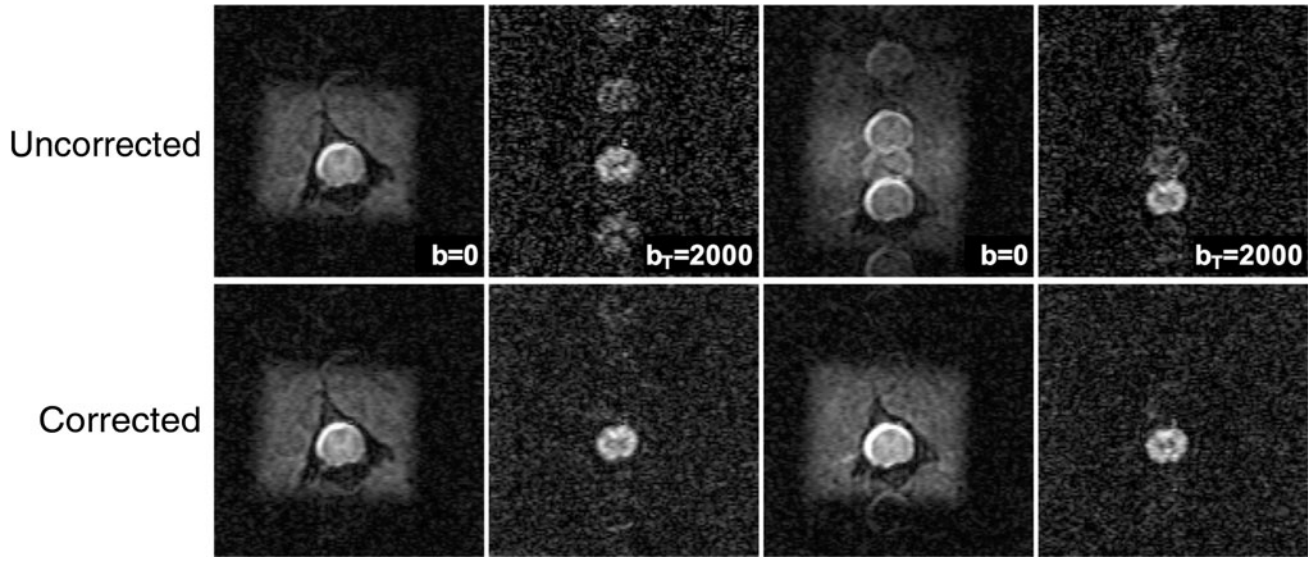

FIG. 2. Echo planar imaging (EPI) artifact phase correction. Ghosting artifacts present in multi-shot diffusion-weighted EPI were evident in both non–diffusion-weighted and diffusion-weighted images (top). The automated phase correction had a negligible effect on artifact free images (A-A′), reduced artifacts caused by motion (B-B′ and D-D′) and corrected phase artifact likely due to motion occurring during the pre-scan EPI calibration (C-C′ and D-D′). Four spatial suppression bands placed outside the cord reduced the contamination from non-cord tissues.

All parameter maps were spatially registered to a common study-specific template space using slice-by-slice iterative registration with Advanced Normalization Tools (ANTS).[37] Fractional anisotropy (FA) and radial diffusivity (RD) maps contain high contrast between white matter (WM), gray matter (GM), and CSF and were jointly used for all registrations. The template was created by registering all images to the initial mean using increasing degrees of freedom from rigid, affine, and non-linear, with six iterations at each step. The spinal cord was straightened along the long axis by aligning the central canal in all slices. Once the template was completed, each dataset was re-registered to the template using a single transformation and interpolation step, and all other DWI parameter maps were similarly transformed. Due to the large slice gap, no interpolation along the slice axis was performed.

Statistical analysis

For all metrics, the maps of mean and coefficient of variation (CoV) were calculated. CoV for each metric was calculated as a ratio of standard deviation over the mean across all sham animals at the first time-point. Regions of interest (ROIs) were manually traced on the template in the white matter, gray matter, and CSF, and ROIs were applied to each of the individual datasets in template space. DTI and FWE ROI values were analyzed for an effect of injury or time by injury interaction using mixed-effect analysis of variance (ANOVA) with injury severity (mild, moderate, severe, and sham) as a fixed effect and time as a repeated factor. Each of the metrics were assessed with a significance threshold of $p < 0.05$.

A linear regression analysis was performed to relate the injury biomechanics (compression) and BBB scores to the DWI metrics. An ROI analysis was first performed at a significance level of $p < 0.05$. Steiger's Z test was used to compare the difference in correlation coefficients between any of the MRI metrics, with BBB scores being a common criterion.[38] For ROIs that had a significant effect of injury severity, a subsequent voxel-wise analysis was performed to visualize the spatial pattern of the relationship. The non-parametric statistical method of randomize with threshold-free cluster enhancement in the FSL[39] was used with a statistical threshold of 0.05 and multiple comparison correction by controlling for the false discovery rate at the voxel level. All statistical analyses were conducted using SPSS (IBM Corp., 2017, Statistical Package for Social Sciences, Version 25.0, Armonk, NY) and Stata (StataCorp, 2011, Stata Statistical Software, Release 12, College Station, TX).

Water content measurement

A separate cohort of animals was used to measure total cord water content in the cord using the dehydration method.[40] Nineteen animals ($n = 10$ sham and $n = 9$ severe) underwent the same contusion injury procedure as described above and were euthanized at the 90-day time-point with 0.22 mL/kg Beuthanasia-D injection (Med-Pharmex, Pomona, CA). The full spinal cord was excised and cut into segments using vertebral bodies as landmarks (C2-T13). The sections were weighed, placed in a 100°C oven for at least 12 h, and weighed again. The percentage of water content lost due to dehydration relative to the initial weight (expressed as %) was calculated for each segment, and the values were averaged across the thoracic and cervical cord segments. A two-sample *t*-test was performed to evaluate changes in water loss between sham and severe groups.

Results

Image processing pipeline

The EPI phase correction reduced the artifacts present in the diffusion and non-diffusion weighted images, with an example shown in Figure 2 that contains both phase correction miscalibration and diffusion weighting phase instability. Both types of artifacts were minimized using the automated procedure. Across all datasets ($n = 122$), phase correction improved the signal in the cord compared with that of the ghost region signal by $5.1\% \pm 2\%$. However, the effect of phase correction on the whole-cord FA values was negligible, $0.99\% \pm 1.7\%$. There was no consistent relationship between either the injury severity or time-point on the degree of EPI artifacts.

Representative single subject and group mean parameter maps are shown in Figure 3. The slice-by-slice spatial registration resulted in the ability to extract white and gray matter ROIs in a predictable and objective way and perform voxel-wise comparisons between subjects. Qualitatively, the free water elimination model alleviated partial volume effects along the spinal cord contour, resulting in a more distinct boundary between white matter and CSF. The improvement was particularly evident in the RD average map. The FWE analysis resulted in reduced CoV in white matter for MD_{FWE} (0.17), RD_{FWE} (0.014), and AD_{FWE} (0.088) compared with DTI metrics MD (0.019), RD (0.019), and AD (0.094). However, the CoV of FA_{FWE} (0.020) was greater than that of FA (0.016). In the gray matter, the CoV of FA_{FWE} (0.40) and RD_{FWE} (0.009) were lower than that of FA (0.047) and RD (0.012). However, the CoV of MD_{FWE} (0.011) and AD_{FWE} (0.049) were larger than that of MD (0.0099) and AD (0.013) in the gray matter. Overall, FWE resulted in a more uniform CoV across all animals, particularly in diffusivity metrics in the white matter.

Group-level ANOVA for main injury effect

Average parameter maps for injury groups at C4, at 90 days, are shown in Figure 4. Average DWI metrics and BBB scores are provided in Supplementary Table 1 (available online at www.liebertpub.com/neu). MD_{FWE}, AD, AD_{FWE}, and FWF_{FWE} showed a tendency to decrease with injury severity at 90 days. A mixed-effects ANOVA showed a significant effect of time for nearly all DTI and FWE indices in white matter: AD [$p = 0.0022$, $F(2,63) = 6.78$], MD [$p = 0.0015$, $F(2,63) = 7.21$], RD [$p = 0.0311$, $F(2,63) = 3.67$], AD_{FWE} [$p = 0.0001$, $F(2,63) = 11.01$], and MD_{FWE} [$p = 0.0004$, $(F(2,63) = 9.04$]. This was similarly seen in gray matter: AD [$p = 0.0155$, $F(2,63) = 4.46$], MD [$p = 0.0057$, $F(2,63) = 5.62$], RD [$p = 0.0050$, $F(2,63) = 5.78$], AD_{FWE} [$p = 0.0008$, $F(2,63) = 8.04$] and MD_{FWE} [$p = 0.0076$, $F(2,63) = 5.28$]. However, an interaction between time and severity was only observed in gray matter AD_{FWE} [$p = 0.0498$, $F(6,63) = 2.25$]. A *post hoc* test for each time-point revealed a significant effect of injury severity only at 90 days post-injury in white matter AD_{FWE} [$p = 0.0414$, $F(3,34) = 3.06$] and MD_{FWE} [$p = 0.0066$, $F(3,34) = 4.83$] and gray matter MD_{FWE} [$p = 0.0088$, $F(3,34) = 4.54$].

Regression analysis

Linear regression analysis between ROI metrics and BBB scores showed consistence with the group analysis, as shown in Table 1. FA, MD_{FWE}, and AD_{FWE} in WM and MD_{FWE} and FWF_{FWE} in GM were significantly associated with locomotor recovery at the 90-day time-point. 90-day AD_{FWE} in white matter was significantly more correlated with 90-day BBB scores than AD ($df = 37$, $Z = 2.2223$, $p < 0.05$). MD and MD_{FWE} in WM ($Z = 1.8226$) and in GM ($Z = 1.3390$) had similar strength correlations. Two- and 30-day post-injury diffusion parameters, however, were not predictive of BBB scores at 90 days.

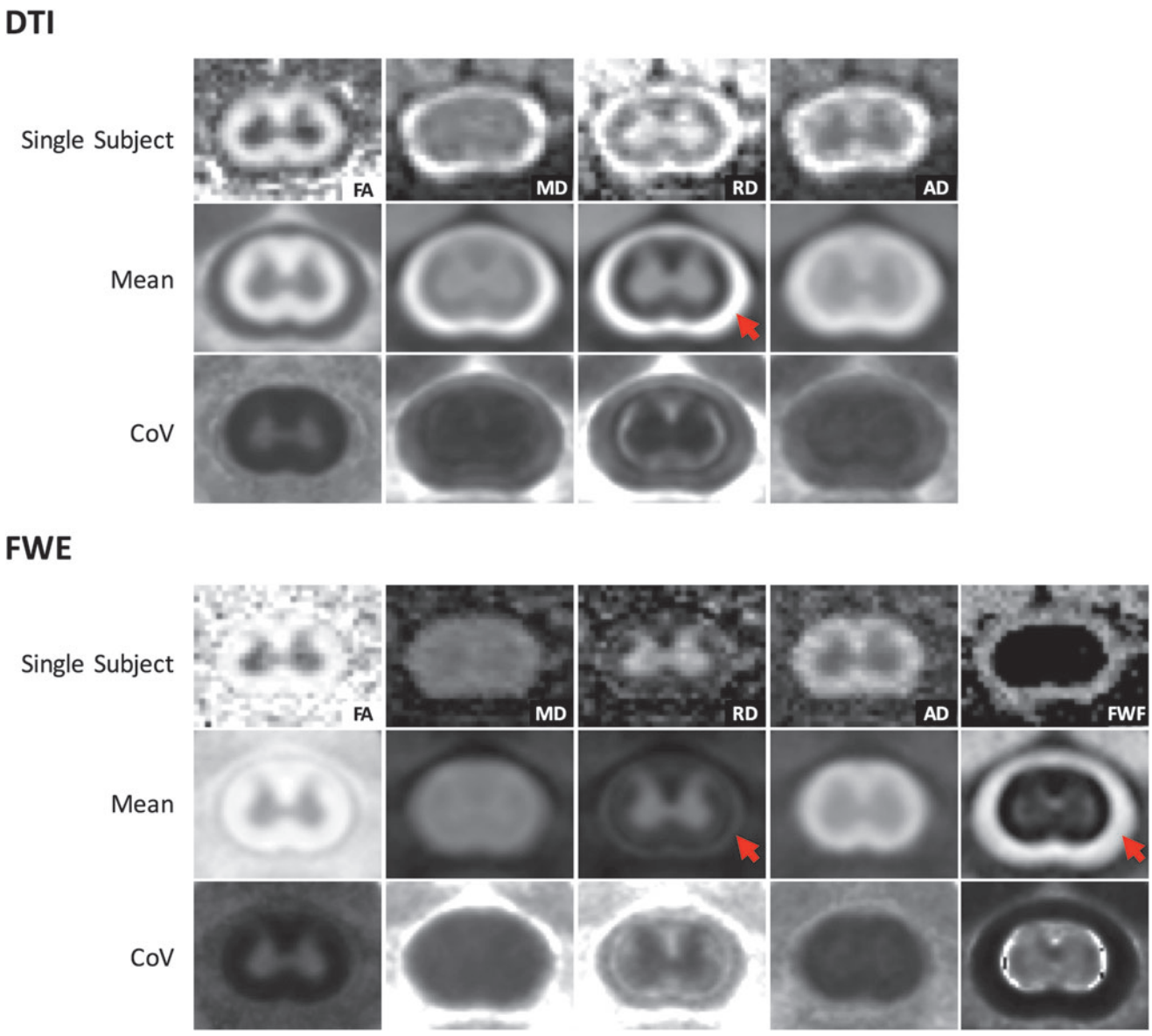

FIG. 3. Mean parameter maps. Registered parameter maps from C4 across all animals demonstrated a reduction of cerebrospinal fluid (CSF) partial volume effects in the free water elimination (FWE) maps compared with diffusion tensor imaging (DTI). The radial diffusivity (RD) map, in particular, showed an improvement in the delineation between the CSF and white matter boundary. The coefficient of variation is more uniform across all animals in the FWE compared with DTI. Color image is available online.

Voxel-wise analysis

Based on the ANOVA and regression with BBB scores, further voxel-wise analysis was performed for metrics showing significant white or gray matter correlations with BBB scores in the ROI analysis. Figure 5 shows the voxels with significant correlations with BBB scores at 90 days post-injury for AD_{FWE}, MD_{FWE}, and FWF_{FWE}. The correlation between BBB and AD_{FWE} was primarily localized in lateral regions of the cervical white matter and was consistently evident across multiple vertebral segments. Significant correlations between BBB score and MD_{FWE} corresponded to similar voxels as AD_{FWE}, but significant voxels also were distributed throughout the gray and white matter and appeared to include the central canal. Significant correlations between BBB score and FWF_{FWE} were evident and predominantly localized to the gray matter, with the voxel near the central canal also showing consistent effects throughout multiple vertebral segments.

Water loss

At 90 days after injury, the wet weights of the severely injured thoracic cord segments were significantly lower than those of the sham cord ($p = 0.002$, $t = 4.519$), as expected given the substantial loss of tissue at the injury site. However, the percent of water lost after dehydration did not significantly differ between sham and severe animals either at the lesion site ($p = 0.442$, $t = -0.893$) or in the cervical cord ($p = 0.298$, $t = 1.256$), as illustrated in Figure 6.

Discussion

Diffusion models and effects of removing free water

The FWE model demonstrated better performance over the standard DTI analysis by both reducing partial volume effects and identifying effects of spinal cord injury remote from the lesion site. Due to the small size of the spinal cord and limited spatial

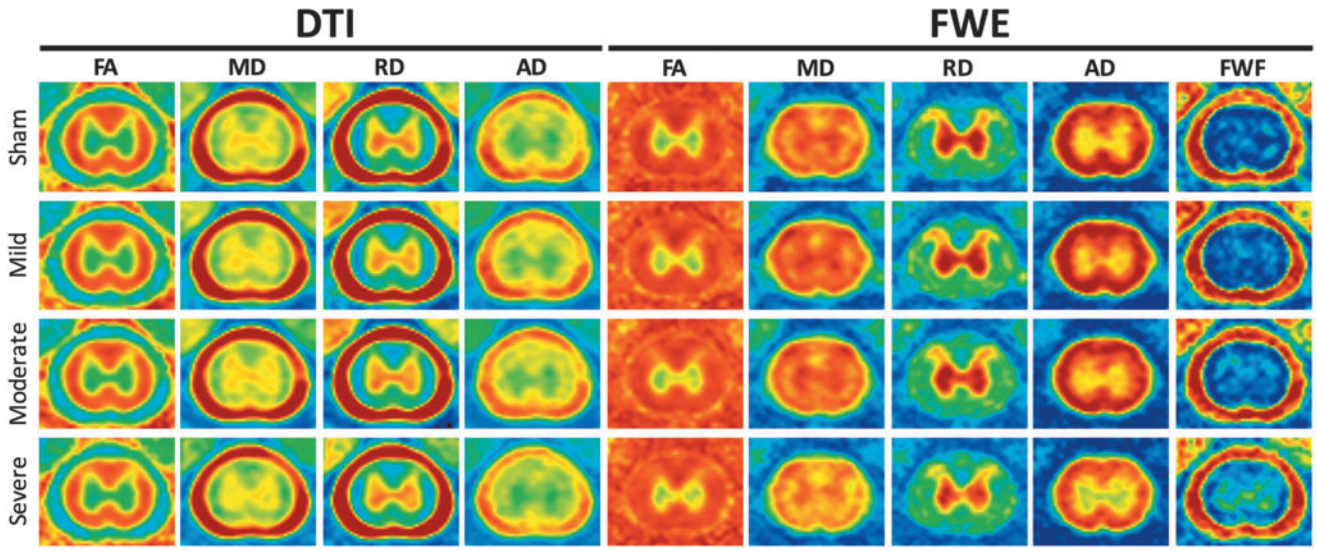

FIG. 4. Diffusion tensor imaging (DTI) and free water fraction (FWF) injury group means at C4 at 90 days. Axial diffusivity using the free water elimination (FWE) model (AD_{FWE}) and mean diffusivity (MD_{FWE}) appear to decrease with injury severity, while FWF_{FWE} increases. DTI parameters do not show a strong relationship to injury severity. Color image is available online.

resolution, partial volume effects are prominent in spinal cord DWI, in which the conventional DTI model tends to underestimate FA and overestimate MD.[20] Hence, the peripheral white matter of the spinal cord has strong partial volume effects that can potentially confound or obscure the effects of contusion injury. The FWE technique removes these free water components, resulting in more accurate diffusion measures along the tissue and CSF boundary. In this study, the AD_{FWE} and MD_{FWE} showed greater sensitivity to injury than DTI metrics in the cervical cord following a thoracic injury. The lack of sensitivity of the DTI model to capture significant diffusion changes *in vivo* may be related to an increase in AD and MD with increased extracellular water/edema that can offset a decreased diffusivity related to axonal damage, as seen in simulation studies.[41] Consistent with the lack of a difference in overall water content in the dehydration experiment, the results suggest a change in water compartmentalization after injury in the cord without a significant difference in overall water content, which is most prominent at the later time-points after injury.

Table 1. Correlations with BBB Scores at 90 DPI

Region	*DWI metric*	R^2	*p value*
WM	FA_{DTI}	0.127	**0.028**
	MD_{DTI}	0.003	0.727
	AD_{DTI}	0.047	0.192
	RD_{DTI}	0.059	0.143
	FA_{FWE}	0.013	0.503
	MD_{FWE}	0.157	**0.014**
	AD_{FWE}	0.136	**0.023**
	RD_{FWE}	0.007	0.880
	FWF_{FWE}	0.089	0.068
GM	FA_{DTI}	0.002	0.792
	MD_{DTI}	0.000	0.914
	MD_{FWE}	0.130	**0.026**
	FA_{FWE}	0.019	0.410
	FWF_{FWE}	0.110	**0.042**

BBB, Basso, Bresnahan, and Beattie scoring scale; DPI, days post-injury; DWI, diffusion-weighted imaging; WM, white matter; GM, gray matter; FA, fractional anisotropy; DTI, diffusion tensor imaging; MD, mean diffusivity; AD, axial diffusivity; RD, radial diffusivity; FWE, free water elimination; FWF, free water fraction.

There is a growing interest in more complex diffusion models that account for free water, as well as other intra-voxel features. The most common approach to reduce the negative effects of CSF uses fluid attenuation inversion recovery. This technique is capable of removing the CSF signal almost completely; however, some of its limitations include reduced signal-to-noise ratio (SNR), higher acquisition time, and difficulty with multi-slice acquisition.[20] Other schemes contain a freely diffusing component; among these are diffusion basis spectrum imaging,[42] neurite orientation distribution diffusion imaging,[43] multiple fascicle models,[44] AxCaliber,[45] and combined hindered and restricted diffusion imaging.[46] However, the complex schemes require long acquisition times and computational power that is currently not easily accessible in the clinic.[19] The FWE model provides additional information to classical DTI model without the need for added scan time and it is already configured for clinical use.[19]

Longitudinal changes: Comparison with ex vivo *data*

Overall, the effects observed with *in vivo* FWE metrics at the later time-points match those previously shown for *ex vivo* DWI studies, but with trends less pronounced than in fixed tissues. *Ex vivo* studies show changes as early as 2 weeks post-injury, with AD and MD remote from the injury decreasing over time compared with controls.[5] In the current study, the 2- and 30-day post-injury time-points exhibited little to no correlation to injury severity. At 10 weeks post-injury, Jirjis and colleagues[7] reported changes in FA, MD, AD, and RD away from the epicenter that were strongly correlated to injury severity. The results in the current study, while significant, were not as prominent as in prior studies of fixed tissues. The discrepancy may be related to changes resulting from aldehyde fixation. Specifically, fixation leads to tissue shrinkage, changes in water relaxation time constants, and water diffusion characteristics.[47] Further, cross-linking between aldehyde and protein

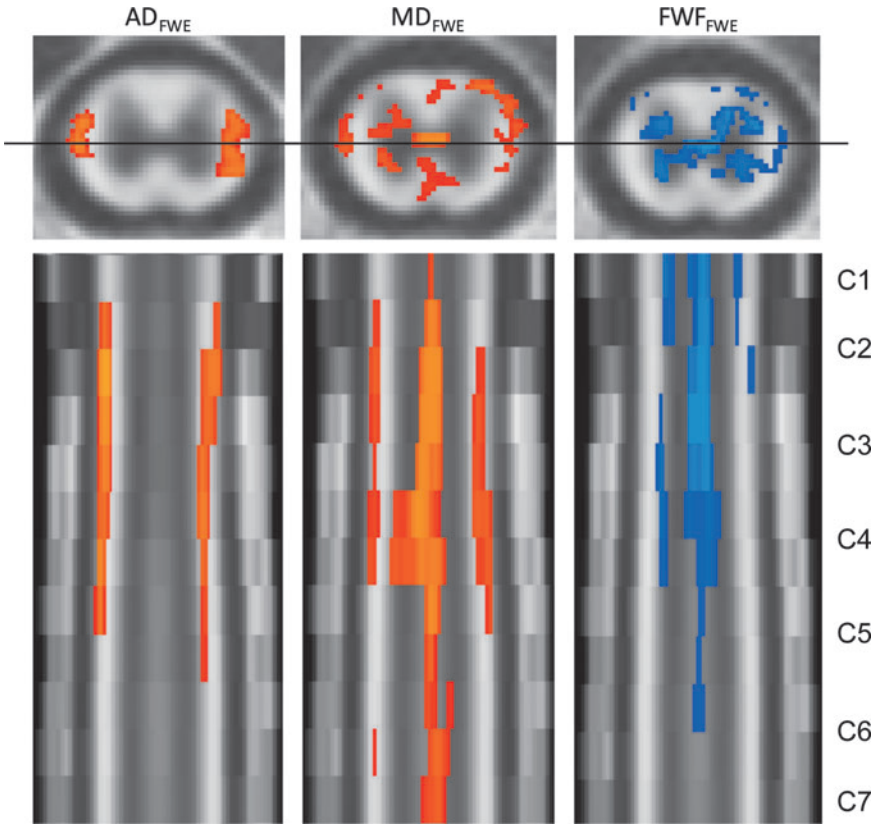

FIG. 5. Correlations with Basso, Bresnahan, and Beattie (BBB) score. At 90 days post-injury, axial diffusivity using the free water elimination (FWE) model (AD_{FWE}), mean diffusivity (MD_{FWE}), and free water fraction (FWF_{FWE}) had significant correlations with BBB score. All significantly correlated pixels (corrected $p < 0.05$) are overlaid onto a template with axial view at C4 (top row) and coronal view of the cervical cord C1-C7 (bottom row). Positive correlations are illustrated in red hues and negative correlations are in blue. MD_{FWE} had a significant positive correlation with BBB score in several regions in the cord. In white matter, a prominent association between BBB score and AD_{FWE} was evident, whereas in the gray matter BBB score was predominantly associated with FWF_{FWE}. Multiple comparison correction was performed at the voxel level by controlling for the false discovery rate. Color image is available online.

molecules is known to form barriers to diffusion.[48] The effect of temperature on diffusion is also a potential factor worth considering. Jirjis and colleagues[7] used a relatively low b-value (500 sec/mm^2) with fixed tissues, which may have sensitized those measurements to different physical features. The current study used a range of b-values between 250 and 2000 sec/mm^2, and although the effects of b-value were not assessed, the prominent difference between these two studies cannot be neglected. While anisotropy is relatively preserved when comparing healthy *in vivo* and *ex vivo* spinal cord tissues,[49] the effects on injured and pathological neurological tissues may not be straightforward, and fixation methods and fixatives may also affect the sensitivity to certain pathological features.[50]

Many structural changes could potentially lead to changes in diffusion, such as axonal degeneration, loss of axons, and demyelination. Previous *in vivo* animal studies have reported a decrease in

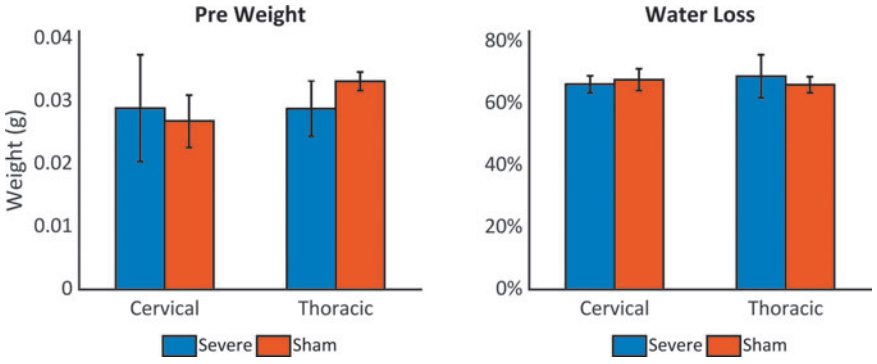

FIG. 6. Percentage of water loss. Average weight of vertebral spinal cord segments before dehydration (left) and mean percentage of water loss (right) at 90 days post-injury. Injured thoracic segments exhibited lower weight than sham samples, but no significant differences in water content were observed. Color image is available online.

AD along with an increase in RD together,[51,52] where AD reflects loss of axonal integrity and RD demyelination.[16,53–55] After a spinal cord injury, AD tends to decrease due to damage to the axons and RD increases since some barriers to diffusion have been destroyed[16,53–55] The relationship between AD and injury is also consistent here; the change in RD, however, is not evident, suggesting axonal damage in the absence of demyelination.[56]

Nonetheless, the *in vivo* changes evident at more chronic (≥ 2 week) time-points in this study are consistent with chronic changes in humans. In humans, MD is significantly lower in chronic SCI subjects across multiple levels of the upper cervical cord[13] compared with healthy controls and is coupled to a decrease in both AD and RD. In the current study, a reduction in both MD and AD was evident, supporting a consistent directionality of the changes. Although no significant RD changes were documented here, the overall trends appear to be constant. The heterogeneity of human SCI, inherent differences between human and rats, and the chronicity of the injury may be the cause of inconsistencies between prior human studies and the current results. Nonetheless, under controlled experimental settings, these results demonstrate consistent and evolving changes in the spinal cord distant from the site of injury detected with DWI.

Relationship between diffusion metrics and locomotor function

Significant relationships were observed between the chronic MRI measures and BBB scores. Voxel-wise analyses revealed a significant positive correlation between AD_{FWE} and BBB scores in the ventrolateral white matter. This is compatible with axonal injury, which has previously been shown to correlate strongly with AD.[56–59] Focal enlargements, also known as neurite beading, are a common feature of Wallerian degeneration and have been implicated in decreased diffusion along white matter tracts.[41] The sensitivity of MD to injury severity appears to be widespread throughout both white and gray matter of the cord, which is consistent with *ex vivo* diffusion data previously observed in our laboratory.[7] Specifically, Jirjis and colleagues[7] reported a strong correlation between *ex vivo* cervical spinal cord (C1-C7) MD and AD measurements and BBB at 10 weeks post-injury. However, these strong *ex vivo* correlations were not observed *in vivo* in the current study.

Several mechanisms could be posited to explain the increase in estimated free water in the gray matter and its strong correlation with injury severity. Previous histologic studies have demonstrated microscopic changes in the gray matter distant from the injury site after SCI. Increased expression of chondroitin sulfate proteoglycans, neurocan, brevican, and neural/glial antigen 2 in the distant dorsal columns was reported after a thoracic injury,[60,61] with the greatest increase occurring at the latest time-point. Additionally, a higher frequency of large motor neurons and a significant decrease in total number of dendrites and branching remote from the site of injury have been previously reported,[62] which could lead to an increase in free water. These microscopic changes and the formation of fluid-filled cavities could lead to changes in free water.

The timeline and mechanics of syrinx formation may also contribute to chronic changes in the cord. Post-traumatic syringomyelia following SCI is a disorder characterized by the development of a progressively expanding fluid-filled cavity within the spinal cord. Surrounded by this astrogliotic wall, the cavities are filled with extracellular fluid and may contain residual macrophages, some connective tissue and blood vessels.[63] While the cavity is most frequently initiated in the gray matter at the injury site, it can extend above and below the lesion and typically occurs in chronic injury.[64–66] The changes in MD and FWF observed in this study do not implicate any single pathological feature. However, they do demonstrate that differences in water compartmentalization may reflect ongoing pathological processes in the injured cord. The lack of a change in bulk edema, as assessed by wet-dry weights in the cervical cord, also highlight the greater sensitivity of DWI compared with gross measures of edema. The results of this study are consistent with results in the human spinal cord demonstrating persistent changes along the entire neuraxis after a localized trauma to the spinal cord.[13,14,67,68] Future studies to address the direct pathological specificity of the changes and potential clinical implications are needed.

Methodological considerations

The preprocessing pipeline and EPI artifact phase correction contributed to creating high-quality data sets by reducing noise and motion artifacts. EPI is susceptible to a Nyquist ghost artifact, which not only degrades image quality and SNR but also can result in inaccurate EPI based quantitative diffusion measurements.[69] Further, these artifacts are exacerbated by higher magnetic fields. Here, the ability to reconstruct images with minimal ghosting artifacts was shown, and even though the phase correction artifact did not improve the quantitative metrics substantially, artifacts caused by motion and scanner miscalibrations were significantly reduced. Spatial registration was found to be improved using slice-by-slice registration. While the spinal cord toolbox[34] has demonstrated regularized slice-wise registration to be acceptable, the animal positioning in this study also included some degree of rotation, which is not corrected using translational or rigid-body transforms. Likewise, the spatial registration allowed regions of interest analysis to be performed in a more consistent and reproducible manner as in previous studies.[70,71] This type of spatial registration could guide future histological studies and allow more direct comparisons between diffusion and histology.

Some limitations of this study are associated with using BBB scoring as the only measure of functional recovery. BBB scoring is subjective, and animals may not move during the short test time. Previous research has shown that minor injuries to the cord may not be reflected in the overall BBB scores.[72] Further, inflammation, incisions, and pain may prevent an accurate BBB evaluation at the early stages of injury.[73] The use of somatosensory evoked potentials may provide a more objective measure of function although it requires additional preparation and instrumentation. Further, biologic biomarkers have also shown promise as predictive biomarkers.[74,75] Imaging signatures and prognostic markers are highly sought given the role imaging already plays in clinical diagnosis.

Conclusions

The FWE technique demonstrated potential for use in evaluating spinal cord injury. It produced a clearer separation between white matter and CSF compared with conventional DTI and showed better sensitivity to locomotor recovery metrics. A strong correlation between BBB and diffusion metrics, AD_{FWE}, MD_{FWE}, and FWF_{FWE}, was observed chronically. Overall, results show that advanced diffusion imaging techniques are sensitive to biological mechanisms of spinal cord injury remote to the epicenter and have the potential to provide imaging biomarkers for clinical diagnosis and management.

Acknowledgments

This project was partially funded through the Research and Education Initiative Fund, a component of the Advancing a Healthier Wisconsin endowment at the Medical College of Wisconsin (MCW), the Craig H. Neilsen Foundation, and the Department of Veterans Affairs. Additional support received from the National Institute of Neurological Disorders and Stroke of the National Institutes of Health under Award Number F31NS096958 (NPS). NPS is a member of the Medical Scientist Training Program at MCW, which is partially supported by a training grant from NIGMS T32-GM080202. This publication was partially supported by the National Center for Advancing Translational Sciences, National Institutes of Health, through grant numbers UL1TR001436 and 1TL1TR001437. Support from the Bryon Riesch Paralysis Foundation is gratefully acknowledged.

Author Disclosure Statement

No competing financial interest exist.

References

1. Burns, A.S., Lee, B.S., Ditunno, J.F., and Tessler, A. (2003). Patient selection for clinical trials: the reliability of the early spinal cord injury examination. J. Neurotrauma 20, 477–82.
2. Fawcett, J.W., Curt, A., Steeves, J.D., Coleman, W.P., Tuszynski, M.H., Lammertse, D., Bartlett, P.F., Blight, A.R., Dietz, V., Ditunno, J., Dobkin, B.H., Havton, L.A., Ellaway, P.H., Fehlings, M.G., Privat, A., Grossman, R., Guest, J.D., Kleitman, N., Nakamura, M., Gaviria, M., and Short, D. (2007). Guidelines for the conduct of clinical trials for spinal cord injury as developed by the ICCP panel: spontaneous recovery after spinal cord injury and statistical power needed for therapeutic clinical trials. Spinal Cord 45, 190–205.
3. Bottomley, P.A., Hardy, C.J., Argensinger, R.E., and Allen-Moore, G. (1987). A review of 1H nuclear magnetic resonance relaxation in pathology: are T1 and T2 diagnostic? Med. Phys. 14, 1–37.
4. Tu, T.W. and Frank, J.A. (2013). Assessing white matter integrity in experimental spinal cord injury using diffusion tensor imaging. J. Neurosci. Neuroengineering 2, 415–430.
5. Ellingson, B.M., Kurpad, S.N., and Schmit, B.D. (2008). Ex vivo diffusion tensor imaging and quantitative tractography of the rat spinal cord during long-term recovery from moderate spinal contusion. J. Magn. Reson. Imaging 28, 1068–1079.
6. Kim, J.H., Loy, D.N., Wang, Q., Budde, M.D., Schmidt, R.E., Trinkaus, K., and Song, S. (2010). Diffusion tensor imaging at 3 hours after traumatic spinal cord injury predicts long-term locomotor recovery. J. Neurotrauma 598, 587–598.
7. Jirjis, M.B., Kurpad, S.N., and Schmit, B.D. (2013). Ex vivo diffusion tensor imaging of spinal cord injury in rats of varying degrees of severity. J. Neurotrauma 30, 1577–1586.
8. Kozlowski, P., Raj, D., Liu, J., Lam, C., Yung, A.C., and Tetzlaff, W. (2008). Characterizing white matter damage in rat spinal cord with quantitative MRI and histology. J. Neurotrauma 25, 653–76.
9. Vedantam, A., Eckardt, G., Wang, M.C., Schmit, B.D., and Kurpad, S.N. (2013). Clinical correlates of high cervical fractional anisotropy in acute cervical spinal cord injury. World Neurosurg. 3–7.
10. Lundell, H., Barthelemy, D., Skimminge, A., Dyrby, T.B., Biering-Sørensen, F., and Nielsen, J.B. (2011). Independent spinal cord atrophy measures correlate to motor and sensory deficits in individuals with spinal cord injury. Spinal Cord 49, 70–75.
11. Ziegler, G., Grabher, P., Thompson, A., Altmann, D., Hupp, M., Ashburner, J., Friston, K., Weiskopf, N., Curt, A., and Freund, P. (2018). Progressive neurodegeneration following spinal cord injury. Neurology 90, e1257–e1266.
12. Ellingson, B.M., Ulmer, J.L., and Schmit, B.D. (2008). Morphology and morphometry of human chronic spinal cord injury using diffusion tensor imaging and fuzzy logic. Ann. Biomed. Eng. 36, 224–236.
13. Ellingson, B.M., Ulmer, J.L., Kurpad, S.N., and Schmit, B.D. (2008). Diffusion tensor MR imaging in chronic spinal cord injury. AJNR Am. J. Neuroradiol. 29, 1976–1982.
14. Freund, P., Weiskopf, N., Ashburner, J., Wolf, K., Sutter, R., Altmann, D.R., Friston, K., Thompson, A., and Curt, A. (2013). MRI investigation of the sensorimotor cortex and the corticospinal tract after acute spinal cord injury: a prospective longitudinal study. Lancet Neurol. 12, 873–881.
15. Becerra, J.L., Puckett, W.R., Hiester, E.D., Quencer, R.M., Marcillo, A.E., Post, M.J.D., and Bunge, R.P. (1995). MR-pathologic comparisons of wallerian degeneration in spinal cord injury. Am. J. Neuroradiol. 16, 125–133.
16. Schwartz, E.D., Chin, C.L., Shumsky, J.S., Jawad, A.F., Brown, B.K., Wehrli, S., Tessler, A., Murray, M., and Hackney, D.B. (2005). Apparent diffusion coefficients in spinal cord transplants and surrounding white matter correlate with degree of axonal dieback after injury in rats. Am. J. Neuroradiol. 26, 7–18.
17. Kelley, B.J., Harel, N.Y., Kim, C.Y., Papademetris, X., Coman, D., Wang, X., Hasan, O., Kaufman, A., Globinsky, R., Staib, L.H., Cafferty, W.B.J., Hyder, F., and Strittmatter, S.M. (2014). Diffusion tensor imaging as a predictor of locomotor function after experimental spinal cord injury and recovery. J. Neurotrauma 31, 1362–1373.
18. Pasternak, O., Sochen, N., Gur, Y., Intrator, N., and Assaf, Y. (2009). Free water elimination and mapping from diffusion MRI. Magn. Reson. Med. 62, 717–730.
19. Hoy, A.R., Koay, C.G., Kecskemeti, S.R., and Alexander, A.L. (2014). Optimization of a free water elimination two-compartment model for diffusion tensor imaging. Neuroimage 103, 323–333.
20. Hoy, A.R., Kecskemeti, S.R., and Alexander, A.L. (2015). Free water elimination diffusion tractography: a comparison with conventional and fluid-attenuated inversion recovery, diffusion tensor imaging acquisitions. J. Magn. Reson. Imaging 42, 1572–1581.
21. Hoy, A.R., Ly, M., Carlsson, C.M., Okonkwo, O.C., Zetterberg, H., Blennow, K., Sager, M.A., Asthana, S., Johnson, S.C., Alexander, A.L., and Bendlin, B.B. (2017). Microstructural white matter alterations in preclinical Alzheimer's disease detected using free water elimination diffusion tensor imaging. PLoS One 12, 1–21.
22. Ofori, E., Pasternak, O., Planetta, P.J., Burciu, R., Snyder, A., Febo, M., Golde, T.E., Okun, M.S., and Vaillancourt, D.E. (2015). Increased free-water in the substantia nigra of Parkinson's disease: a single-site and multi-site study. Neurobiol. Aging 36, 1097–1104.
23. Rydhög, A.S., Szczepankiewicz, F., Wirestam, R., Ahlgren, A., Westin, C.F., Knutsson, L., and Pasternak, O. (2017). Separating blood and water: perfusion and free water elimination from diffusion MRI in the human brain. Neuroimage 156, 423–434.
24. Metz, G.A., Curt, A., van de Meent, H., Klusman, I., Schwab, M.E., and Dietz, V. (2000). Validation of the weight-drop contusion model in rats: a comparative study of human spinal cord injury. J. Neurotrauma 17, 1–17.
25. Gruner, J.A. (1992). A monitored contusion model of spinal cord injury in the rat. J. Neurotrauma 9, 123–126.
26. Young, W. (2009). MASCIS spinal cord contusion model, in: *Animal Models of Acute Neurological Injuries,* J. Chen, Z.C. Xu, X.M. Xu, and J.H. Zhang. (eds). Humana Press: New York, NY, pps. 1–498.
27. Young, W. (2002). Spinal cord contusion models. Prog. Brain Res. 137, 231–255.
28. Basso, D.M., Beattie, M.S., and Bresnahan, J.C. (1995). A sensitive and reliable locomotor rating scale for open field testing in rats. J. Neurotrauma 12, 1–21.
29. Basso, D.M., Beattie, M.S., and Bresnahan, J.C. (1996). Graded histological and locomotor outcomes after spinal cord contusion using the NYU weight-drop device versus transection. Exp. Neurol. 139, 244–256.
30. Zakszewski, E., Schmit, B., Kurpad, S.N., and Budde, M.D. (2015). Diffusion imaging in the rat cervical spinal cord. J. Vis. doi: 10.3791/52390.
31. Gomori, J.M., Holland, G.A., Grossman, R.I., Gefter, W.B., and Lenkinski, R.E. (1988). Fat suppression by section-select gradient reversal on spin-echo MR imaging. Work in progress. Radiology 168, 493–495.
32. Hasan, K.M., Parker, D.L., and Alexander, A.L. (2001). Comparison of gradient encoding schemes for diffusion-tensor MRI. J. Magn. Reson. Imaging 13, 769–780.
33. Chen, N.K., Avram, A.V., and Song, A.W. (2011). Two-dimensional phase cycled reconstruction for inherent correction of echo-planar imaging nyquist artifacts. Magn. Reson. Med. 66, 1057–1066.
34. De Leener, B., Lévy, S., Dupont, S.M., Fonov, V.S., Stikov, N., Louis Collins, D., Callot, V., and Cohen-Adad, J. (2017). SCT: Spinal Cord Toolbox, an open-source software for processing spinal cord MRI data. Neuroimage 145, 24–43.

35. Andersson, J.L.R. and Sotiropoulos, S.N. (2016). An integrated approach to correction for off-resonance effects and subject movement in diffusion MR imaging. Neuroimage 125, 1063–1078.
36. Basser, P.J., Mattiello, J., and Le Bihan, D. (1994). Estimation of the effective self-diffusion tensor from the NMR spin echo. J. Magn. Reson. B 103, 247–254.
37. Avants, B.B., Tustison, N.J., Stauffer, M., Song, G., Wu, B., and Gee, J.C. (2014). The Insight ToolKit image registration framework. Front. Neuroinform. 8, 1–13.
38. Steiger, J.H. (1980). Tests for comparing elements of a correlation matrix. Psychol. Bull. 87, 245–251.
39. Jenkinson, M., Beckmann, C.F., Behrens, T.E.J., Woolrich, M.W., and Smith, S.M. (2012). FSL. Neuroimage 62, 782–790.
40. Adachi, M. and Feigin, I. (1966). Cerebral oedema and the water content of normal white matter. J. Neurol. Neurosurg. Psychiatry 29, 446–450.
41. Skinner, N.P., Kurpad, S.N., Schmit, B.D., and Budde, M.D. (2015). Detection of acute nervous system injury with advanced diffusion-weighted MRI: a simulation and sensitivity analysis. NMR Biomed. 28, 1489–1506.
42. Wang, Y., Wang, Q., Haldar, J.P., Yeh, F.C., Xie, M., Sun, P., Tu, T.W., Trinkaus, K., Klein, R.S., Cross, A.H., and Song, S. (2011). Quantification of increased cellularity during inflammatory demyelination. Brain 134, 3590–3601.
43. Zhang, H., Schneider, T., Wheeler-Kingshott, C.A., and Alexander, D.C. (2012). NODDI: practical in vivo neurite orientation dispersion and density imaging of the human brain. Neuroimage 61, 1000–1016.
44. Scherrer, B., and Warfield, S.K. (2012). Parametric representation of multiple white matter fascicles from cube and sphere diffusion MRI. PLoS One 7.
45. Barazany, D., Basser, P.J., and Assaf, Y. (2009). In vivo measurement of axon diameter distribution in the corpus callosum of rat brain. Brain 132, 1210–1220.
46. Assaf, Y., Freidlin, R.Z., Rohde, G.K., and Basser, P.J. (2004). New modeling and experimental framework to characterize hindered and restricted water diffusion in brain white matter. Magn. Reson. Med. 52, 965–978.
47. Sun, S.W., Neil, J.J., and Song, S. (2003). Relative indices of water diffusion anisotropy are equivalent in live and formalin-fixed mouse brains. Magn. Reson. Med. 50, 743–748.
48. Pattany, P.M., Puckett, W.R., Klose, K.J., Quencer, R.M., Bunge, R.P., Kasuboski, L., and Weaver, R.G. (1997). High-resolution diffusion-weighted MR of fresh and fixed cat spinal cords: Evaluation of diffusion coefficients and anisotropy. Am. J. Neuroradiol. 18, 1049–1056.
49. Madi, S., Hasan, K.M., and Narayana, P.A. (2005). Diffusion tensor imaging of in vivo and excised rat spinal cord at 7 T with an icosahedral encoding scheme. Magn. Reson. Med. 53, 118–125.
50. Schwartz, E.D., Cooper, E.T., Chin, C.L., Wehrli, S., Tessler, A., and Hackney, D.B. (2005). Ex vivo evaluation of ADC values within spinal cord white matter tracts. AJNR Am. J. Neuroradiol. 26, 390–397.
51. Sundberg, L.M., Herrera, J.J., and Narayana, P.A. (2010). In vivo longitudinal MRI and behavioral studies in experimental spinal cord injury. J. Neurotrauma 27, 1753–1767.
52. Cohen-Adad, J., El Mendili, M.M., Lehéricy, S., Pradat, P.-F., Blancho, S., Rossignol, S., and Benali, H. (2011). Demyelination and degeneration in the injured human spinal cord detected with diffusion and magnetization transfer MRI. Neuroimage 55, 1024–1033.
53. DeBoy, C.A., Zhang, J., Dike, S., Shats, I., Jones, M., Reich, D.S., Mori, S., Nguyen, T., Rothstein, B., Miller, R.H., Griffin, J.T., Kerr, D.A., and Calabresi, P.A. (2007). High resolution diffusion tensor imaging of axonal damage in focal inflammatory and demyelinating lesions in rat spinal cord. Brain 130, 2199–2210.
54. Schwartz, E.D., Cooper, E.T., Fan, Y., Jawad, A.F., Chin, C.-L., Nissanov, J., and Hackney, D.B. (2005). MRI diffusion coefficients in spinal cord correlate with axon morphometry. Neuroreport 16, 73–76.
55. Ford, J.C., Hackney, D.B., Alsop, D.C., Jara, H., Joseph, P.M., Hand, C.M., and Black, P. (1994). MRI characterization of diffusion coefficients in a rat spinal cord injury model. Magn. Reson. Med. 31, 488–494.
56. Song, S., Sun, S.-W., Ju, W.K., Lin, S.J., Cross, A.H., and Neufeld, A.H. (2003). Diffusion tensor imaging detects and differentiates axon and myelin degeneration in mouse optic nerve after retinal ischemia. Neuroimage 20, 1714–1722.
57. Schwartz, E.D., and Hackney, D.B. (2003). Diffusion-weighted MRI and the evaluation of spinal cord axonal integrity following injury and treatment. Exp. Neurol. 184, 570–589.
58. Kim, J.H., Budde, M.D., Liang, H.F., Klein, R.S., Russell, J.H., Cross, A.H., and Song, S. (2006). Detecting axon damage in spinal cord from a mouse model of multiple sclerosis. Neurobiol. Dis. 21, 626–632.
59. Budde, M.D., Xie, M., Cross, A.H., and Song, S. (2009). Axial diffusivity is the primary correlate of axonal injury in the experimental autoimmune encephalomyelitis spinal cord: a quantitative pixelwise analysis. J. Neurosci. 29, 2805–2813.
60. Massey, J.M., Amps, J., Viapiano, M.S., Matthews, R.T., Wagoner, M.R., Whitaker, C.M., Alilain, W., Yonkof, A.L., Khalyfa, A., Cooper, N.G.F., Silver, J., and Onifer, S.M. (2008). Increased chondroitin sulfate proteoglycan expression in denervated brainstem targets following spinal cord injury creates a barrier to axonal regeneration overcome by chondroitinase ABC and neurotrophin-3. Exp. Neurol. 209, 426–445.
61. Andrews, E.M., Richards, R.J., Yin, F.Q., Viapiano, M.S., and Jakeman, L.B. (2012). Alterations in chondroitin sulfate proteoglycan expression occur both at and far from the site of spinal contusion injury. Exp. Neurol. 235, 174–187.
62. Bose, P., Parmer, R., Reier, P.J., and Thompson, F.J. (2005). Morphological changes of the soleus motoneuron pool in chronic midthoracic contused rats. Exp. Neurol. 191, 13–23.
63. Norenberg, M.D., Smith, J., and Marcillo, A. (2004). The pathology of human spinal cord injury: defining the problems. J. Neurotrauma 21, 429–440.
64. Umbach, I. and Heilporn, A. (1991). Review article: post-spinal cord injury syringomyelia. Paraplegia 29, 219–221.
65. Schurch, B., Wichmann, W., and Rossier, A.B. (1996). Post-traumatic syringomyelia (cystic myelopathy): a prospective study of 449 patients with spinal cord injury. J. Neurol. Neurosurg. Psychiatry 60, 61–67.
66. Williams, B. (1990). Post-traumatic syringomyelia, an update. Paraplegia 28, 296–313.
67. Petersen, J.A., Wilm, B.J., von Meyenburg, J., Schubert, M., Seifert, B., Najafi, Y., Dietz, V., and Kollias, S. (2012). Chronic cervical spinal cord injury: DTI correlates with clinical and electrophysiological measures. J. Neurotrauma 29, 1556–1566.
68. Shanmuganathan, K., Gullapalli, R.P., Zhuo, J., and Mirvis, S.E. (2008). Diffusion tensor MR imaging in cervical spine trauma. Am. J. Neuroradiol. 29, 655–659.
69. Porter, D.A., Calamante, F., Gadian, D.G., and Connelly, A. (1999). The effect of residual Nyquist ghost in quantitative echo-planar diffusion imaging. Magn. Reson. Med. 42, 385–392.
70. Smith, A.C., Weber, K.A., O'Dell, D.R., Parrish, T.B., Wasielewski, M., and Elliott, J.M. (2018). Lateral corticospinal tract damage correlates with motor output in incomplete spinal cord injury. Arch. Phys. Med. Rehabil. 99, 660–666.
71. Martin, A.R., De Leener, B., Cohen-Adad, J., Cadotte, D.W., Kalsi-Ryan, S., Lange, S.F., Tetreault, L., Nouri, A., Crawley, A., Mikulis, D.J., Ginsberg, H., and Fehlings, M.G. (2017). A novel MRI biomarker of spinal cord white matter injury: T2*-weighted white matter to gray matter signal intensity ratio. Am. J. Neuroradiol. 38, 1266–1273.
72. Agrawal, G., Kerr, C., Thakor, N. V, and All, A.H. (2011). Characterization of graded MASCIS contusion spinal cord injury using somatosensory evoked potentials. Spine (Phila. Pa. 1976). 35, 1122–1127.
73. Agrawal, G., Thakor, N. V., and All, A.H. (2009). Evoked potential versus behavior to detect minor insult to the spinal cord in a rat model. J. Clin. Neurosci. 16, 1052–1055.
74. Kwon, B.K., Streijger, F., Fallah, N., Noonan, V.K., Bélanger, L.M., Ritchie, L., Paquette, S.J., Ailon, T., Boyd, M.C., Street, J., Fisher, C.G., and Dvorak, M.F. (2017). Cerebrospinal fluid biomarkers to stratify injury severity and predict outcome in human traumatic spinal cord injury. J. Neurotrauma 34, 567–580.
75. Pouw, M.H., Kwon, B.K., Verbeek, M.M., Vos, P.E., Van Kampen, A., Fisher, C.G., Street, J., Paquette, S.J., Dvorak, M.F., Boyd, M.C., Hosman, A.J.F., and Van De Meent, H. (2014). Structural biomarkers in the cerebrospinal fluid within 24 h after a traumatic spinal cord injury: a descriptive analysis of 16 subjects. Spinal Cord 52, 428–433.

Address correspondence to:
Alice Motovylyak, BS
Department of Biomedical Engineering
Marquette University/Medical College of Wisconsin
Olin Engineering Center, Room 206
1515 West Wisconsin Avenue
Milwaukee, WI 53233

E-mail: olesya.motovylyak@marquette.edu